Journal of Engineering for Gas Turbines and Power. Received March 27, 2021;
Accepted manuscript posted July 29, 2021. doi:10.1115/1.4051951

Numerical and Experimental Study on the Impact of Mild Cold EGR on Exhaust Emissions in a Biodiesel Fueled Diesel Engine

Alex de Oliveira,[1] Junfeng Yang[2] and José Ricardo Sodré[3]*

* Email address of corresponding author: J.Yang@leeds.ac.uk

[1] Department of Mechanical Engineering, Pontifical Catholic University of Minas Gerais, Belo Horizonte, 30535-610, Brazil.

[2] School of Mechanical Engineering, Institute, University of Leeds, Leeds, LS2 9JT, UK.

[3]College of Engineering and Physical Sciences, Aston University, Aston St, Birmingham B4 7ET, UK.

ABSTRACT: This work evaluated the effect of cooled exhaust gas recirculation (EGR) on fuel consumption and pollutant emissions from a diesel engine fueled with B8 (a blend of biodiesel and No. Diesel 8:92% by volume), experimentally and numerically. Experiments were carried out on a Diesel power generator with varying loads from 5 kW to 35 kW and 10% of cold EGR ratio. Exhaust emissions (e.g. Total Hydrocarbons (THC), Nitrogen Oxides (NOx), Carbon Monoxide (CO) etc.) were measured and evaluated. The results showed mild EGR and low biodiesel content have minor impact of engine specific fuel consumption, fuel conversion efficiency and in-cylinder

Journal of Engineering for Gas Turbines and Power. Received March 27, 2021;
Accepted manuscript posted July 29, 2021. doi:10.1115/1.4051951

pressure. Meanwhile, the combination of EGR and biodiesel reduced THC and NOx up to 52% and 59%, which shows promising effect on overcoming the Particulate Matter (PM) -NOx trade-off from diesel engine. A 3-Dimensional (3D) Computational Fluid Dynamics (CFD) engine model incorporated with detailed biodiesel combustion kinetics and NOx formation kinetics was validated against measured in-cylinder pressure, temperature and engine-out Nitric Oxide (NO) emission from diesel engine. This valid model was then employed to investigate the in-cylinder temperature and equivalence ratio distribution that predominate NOx formation. The critical results showed that the reduction of NOx emission by EGR and biodiesel is obtained by a little reduction of the local in-cylinder temperature and, mainly, by creating comparatively rich combusting mixture which makes the combustion path pass through lower NOx zone in the ϕ-T diagram.

KEYWORDS: Biodiesel, Exhaust Gas Recirculation, Nitrogen Oxides, Computational Fluid Dynamics, Engine measurement

1. INTRODUCTION

Over the last decades, the allowable limits of internal combustion engine pollutant emissions has been reduced, as a consequence of continuous growth of environmental pollution and increasing concern for the environment and air quality (Oliveira et al. 2018; Hosseinzadeh-Bandbafha et al. 2018). Therefore, replacing conventional diesel fuels with clean and renewable fuels, e.g. biodiesel, bioethanol, has become an urgent matter.

Biodiesel is commonly derived from vegetable oil, or animal fat, or used edible oils via transesterification reactions (Balamurugan et al. 2018). Biodiesels consist of long chain methyl or ethyl esters, which have similar liquid and thermochemical properties as those of conventional

diesel. This allows it to be used in place of conventional diesel without having to significantly modify the engine hardware. In addition, biodiesels have higher Cetane numbers than conventional diesel (Giakoumis and Sarakatsanis 2019) and thus ignite more readily. This favors combustion phasing and yields a higher combustion efficiency.

Engines fuelled by biodiesel generate relatively low emissions of several key pollutants in the exhaust (US EPA 2002; Graboski and McCormick 1998; Knothe, Krahl, Gerpen 2005). Moreover, biodiesel has excellent lubricity properties and high flash point, making it safer to store (Knothe, Krahl, Gerpen 2005; Knothe 2008). However, biodiesel has a lower specific energy content than diesel oil. It usually results in a relative higher fuel consumption rate and lower brake thermal efficiency when used for diesel engines (Çelik 2017; Çelik and Özgören 2017). Other disadvantages of using biodiesel include relatively high emissions of nitrogen oxides exhaust (US EPA 2002; Lapuerta et al. 2008), decreased oxidative stability, worse cold-flow performance than petroleum diesel, and dilution of lubricating fluids (Andreae et al. 2007) due to fuel impingement on in-cylinder surfaces when early- or late- injection strategies are employed for diesel engines.

Nitrogen oxides (NOx) are toxic to human beings and harmful to the environment and therefore subject to more stringent regulations to limit their emissions from engines. A majority of NOx formation are governed by combustion temperature (Zel'dovich et al. 1947). Therefore, many strategies for controlling engine-out NOx emissions have been developed based on low temperature combustion concept (Shin et al. 2011; Palash et al. 2013). For example, cooled exhaust gas recirculation (EGR), water injection, and injection timing retardation. Cooled EGR has been proven effective in reducing NOx emission from internal combustion engines (Bozza et al. 2016; Edara et al. 2018; Divekar et al. 2016). Several studies showed that this reduction results from thermal, chemical and dilution effects (Ladommatos et al. 1997). Whereas, the use of EGR causes

the increase of particulate matter (PM) emissions, known as PM-NOx trade-off. Asad et al. (2015) developed a Premixed Pilot Assisted Combustion strategy to reduce NOx and soot simultaneously from a diesel engine fitted with EGR, in which ported injected ethanol is ignited by a single diesel pilot injection at Top Dead Centre (TDC). The use of diesel engine on dual fuel mode, blending diesel oil or biodiesel with n-butanol, coupled with EGR seems to be effective to overcome the PM-NOx trade-off (Zheng et al. 2018). Although engine experiments have been widely conducted to explore the possibility of reducing NOx and PM using a combination of EGR and biodiesel (Muncrief et al. 2008; Jothithirumal and Jamesgunasekaran 2012), the underlying mechanism of emission reduction is not fully understood yet due to limited information on in-cylinder combustion phasing and flow pattern, emission formation/oxidation zones. Ideally, optical engine measurement with advanced laser diagnostics should be performed to obtain this information. However, such experiments are generally expensive, time-consuming and the results require very specific knowledge to interpret, and therefore, there are comparatively few literature reports describing optical biodiesel engine with EGR loads.

The rapid development of computer technology and numerical models has made it possible to obtain useful predictions on sprays, auto-ignition and reactive flow in engines. Several CFD codes, e.g. KIVA code family, FORTE, FIRE, STAR-CD, OpenFOAM and CONVERGE have been developed to perform multidimensional simulations on combustion engines, such as fuel variability (Huang et al. 2016), EGR impact (Kumar et al. 2017), knock resistance (Boccardi et al. 2016), soot formation (Naik et al. 2013), dual fuels (Fraioli et al. 2014; Huang et al. 2015; Dong et al. 2016), injection strategies (Cameretti et al. 2016) and fuel sprays (Wei et al. 2014; Das and Lim 2017). Yang et al. (2012) studied the effects of the start of injection (SOI) and EGR on a biodiesel engine performance using a reduced combustion kinetics implemented in ANSYS Forte

CFD simulation package. Mardi et al. (2014) investigated the effects of EGR on the emissions and performance of a spark ignition engine using AVL FIRE CFD code to solve the flow field equations for the closed cycle of the engine. Both numerical simulations predicted significant NOx reduction using EGR. However, there are comparatively few literature reports describing numerical modelling on biodiesel engine because of the complexity of biodiesel oxidation. Previous work had focused on global or reduced mechanisms involving fewer reactions and species. The engine validation on these biodiesel combustion models is rarely achieved. The route of NOx formation/oxidation in biodiesel engine has not been completely examined. Moreover, the interaction between EGR and biodiesel on NOx remains unclear.

An improved understanding on NOx emissions of biodiesel engine with EGR could lead to inexpensive and effective mitigation strategies to overcome the PM-NOx trade-off. The objective of the present study is to extend previous work to gain deeper insights into the route of NOx formation in engines through a valid biodiesel combustion model. Therefore, this work first presents experimental results of a diesel engine fueled with B8 (a blend of biodiesel and Diesel 8:92% by volume) and 10% of cold EGR, including performance and emissions data. A 3D biodiesel engine model has been constructed using ANSYS Forte software and validated against those experimental data. Then a wide range of engine simulations using this valid biodiesel model have been performed to obtain a better understanding on the impact of biodiesel and EGR on the formation of NOx.

The rest of this paper is organized as follows. In Section 2, we present the details of experimental setup and numerical model. A discussion of our results is provided in Section 3. Finally, Section 4 is devoted to concluding remarks.

2. MATERIALS AND METHODS

2.1 Experimental Methodology

The experimental and numerical studies were conducted based on a production, naturally-aspirated, four-stroke, four-cylinder diesel engine, with the main characteristics present in Table 1.

Table 1. Diesel engine specifications.

Manufacture/Type	MWM 229/4
Cycle	Four-stroke
Diesel oil injection	Direct
Bore × stroke	102 mm × 120 mm
Number of cylinders	4, in line
Compression ratio	17:1
Total displacement	3.922 L
Rated Power	44 kW
Intake system	Naturally aspirated
Start of injection	23°Before TDC

This diesel engine is equipped with a mechanically controlled injection system and the fuel injection settings remains un-changed during the studies. The diesel injector has four holes with diameter of 0.3 mm. For recirculation of the exhaust gas, an appropriate pipeline was installed with a water cooling heat exchanger. The EGR quantity was regulated by an electric valve installed in the EGR loop. An electronic system was developed to keep the EGR rate (%) fixed at 10%, controlling the valve position, and the intake air temperature at 40°C, when using EGR, controlling the cooling water flow. The different EGR valve positions were previously related to the EGR rate (%) for various engine loads. The EGR rate was determined comparing the carbon dioxide (CO_2) concentrations in the engine exhaust and intake, since the fresh air contains negligible amounts of CO_2. The measurement of CO_2 was obtained from two taps built in the intake and exhaust manifolds to sample the gas.

Journal of Engineering for Gas Turbines and Power. Received March 27, 2021;
Accepted manuscript posted July 29, 2021. doi:10.1115/1.4051951

The main measured parameters during the experiments were: temperature in different positions, fuel consumption, intake air mass flow rate and humidity, ambient conditions, engine load, CO_2, CO, O_2, THC, NO, NOx emissions and in-cylinder pressure. All experimental data were acquired by a data and acquisition system built in LabVIEW platform. The layout of test cell is shown in Figure 1 and the measurement device specifications are available in the Appendix A.

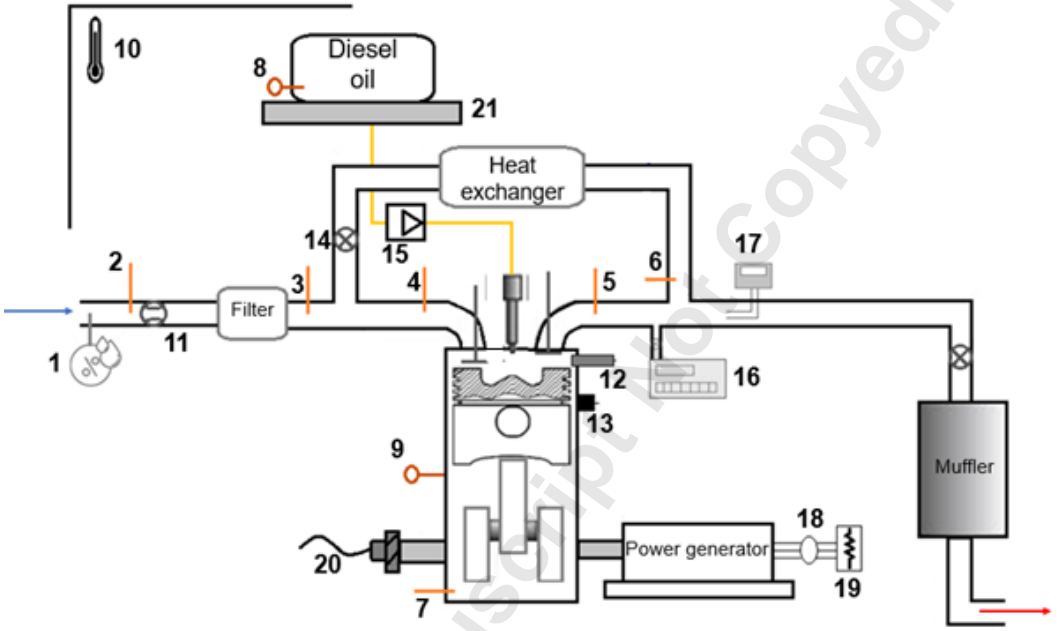

1	Thermohygrometer	8	Thermoresistor: diesel oil	15	Diesel oil mechanical pump
2	Thermocouple: fresh air	9	Thermoresistor: cooling water	16	Gas analyser
3	Thermocouple: fresh air	10	Barometer: atmospheric pressure	17	Opacimeter
4	Thermocouple: fresh air + exhaust gas	11	Mass airflow sensor	18	Power transducer
5	Thermocouple: exhaust gas	12	In-cylinder pressure sensor	19	Load bank
6	Thermocouple: recirculated gas	13	Knock sensor	20	Encoder
7	Thermocouple: crankcase oil	14	EGR valve	21	Platform balance

Figure 1. Schematics of the experimental apparatus.

The tests were conducted using B8 fuel required by Brazilian government law No. 13263 (2016), which established the compulsory addition of biodiesel to diesel oil to 8% from March 2017. The fuel properties (density, viscosity, Cetane number, lower heating value, etc.) of B8 meets the ANP specifications (see ANP Resolution No.45/2014). Common biodiesels include Rapeseed Methyl Ester (RME), Soybean Methyl Ester (SME), and Palm Methyl Ester (PME). At present, approximately 70% of biodiesel produced in Brazil is derived from soybeans. The average compositions (% by volume) of soybean-derived biodiesel, SME, is provided in Table 2. In addition, the key specifications of diesel oil, SME and B8 are given in Table 3. The tests were conducted without the EGR system (B8) and with 10% of EGR rate (B8 + EGR). Three tests were conducted for each engine condition, varying the engine loads from 5 kW to 35 kW and according to ISO 3046-1:2002 standard. The readings at each test were performed after the engine reached the steady-state condition, observing the exhaust gas and the cooling water temperatures. The load power and fuel consumption results were corrected to ambient standard conditions. The average results are presented, and the combined standard uncertainty of the results is a combination of both the statistical spread and the instrument uncertainty.

Table 2. The average compositions (% by volume) of soybean-derived biodiesel, SME.

Esters	Formulas	% by vol.
Methyl palmitate	$C_{17}H_{34}O_2$	6-10
Methyl stearate	$C_{19}H_{38}O_2$	2-5
Methyl oleate	$C_{19}H_{36}O_2$	20-30
Methyl linoleate	$C_{19}H_{34}O_2$	50-60

Methyl linolenate	$C_{19}H_{32}O_2$	50-11

Table 3. Key specifications for Brazil diesel fuel S10, Soybean-derived biodiesel, SME, and a blend of S10 and SME, B8.

Property	Diesel S10	Diesel S10 B8	SME
Density, kg/m^3	839.4	843	883.3
Kinematic Viscosity, mm^2/s	2.85	2.96	4.22
Flash point, °C	38	38	159
Cloud point, °C	-5	-5	-3
Cetane number	50	50	50.4
Lower heating value, MJ/kg	42.7	42.2	37.3

2.2 NUMERICAL METHODOLOGY

To handle the spray combustion process in diesel engine, there are three physical steps that need to be considered in numerical modelling: the turbulent gas phase flow (gas phase modeling and turbulence modeling), the transformation of the injected liquid fuel into a gaseous state (spray modeling), and the subsequent combustion of the fuel vapor in the presence of a gaseous oxidizer (combustion modeling). The first of these stages usually involves a set of governing equations (mass, momentum and energy conservations) and turbulence model, and the reliability of the simulation will depend on the quality of this model. The second stage involves a number of models: a spray breakup model that describes primary and secondary breakup, droplet collision/evaporation models, and a droplet-turbulence interaction model. The third stage involves modeling complex chemical reactions taking place in turbulent media. The governing equations

(Eqs. 1-4) for these three physical steps are formulated to solve the ensemble-averaged flow field in the Reynolds-averaged Navier–Stokes (RANS) approach.

The conservation equation for the mass of species *m* is expressed as

$$\frac{\partial \rho_m}{\partial t} + \nabla \cdot (\rho_m \mathbf{u}) = \nabla \cdot \left[\rho D \nabla \left(\frac{\rho_m}{\rho}\right)\right] + \dot{\rho}_m^c + \dot{\rho}^s \delta_{ml} \quad (1)$$

where $\dot{\rho}_m$is the mass density of species *m*, ρ is the total mass density, and **u** is the fluid velocity vector, ∇ is the vector operator, *D* is the mass diffusion coefficient estimated using Fick's law, $\dot{\rho}_m^c$ is the chemistry source term originating from the chemical reaction given. $\dot{\rho}^s$ is the rate of mass exchange due to the evaporation of liquid to the gas-phase, and δ_{ml} is the Dirac delta function for species *l*, of which the spray droplets are composed.

Because mass is conserved during chemical reactions, summing the outputs of Eq. 1 for all species involved in the combustion process gives the overall mass conservation, Eq. 2.

$$\frac{\partial \rho}{\partial t} + \nabla \cdot (\rho \mathbf{u}) = \dot{\rho}^s \quad (2)$$

The momentum equation for the fluid mixture is

$$\frac{\partial \rho \mathbf{u}}{\partial t} + \nabla \cdot (\rho \mathbf{u}\mathbf{u}) = -\nabla p - \frac{2}{3}\nabla(\rho k) + \nabla \cdot \sigma + \mathbf{F}^s + \rho g \quad (3)$$

where *p* is the fluid pressure and can be calculated using the equation of state for a mixture of ideal gases, *σ* is the viscous stress tensor and accounts for the surface stress caused by fluid motion. It can be calculated once the turbulent viscosity, μ_t, is known. Re-Normalization Group (RNG) *k*-*ε* model in which μ_t is correlated to the turbulent kinetic energy, *k*, and the turbulent dissipation rate, *ε*, has been employed in this work. Solving these two transport equations (i.e. the *k*-equation and the *ε*-equation) makes it possible to compute μ_t, which in turn makes it possible to obtain the viscous stress tensor, *σ*. $\mathbf{F}^s$ is the rate of momentum gain per unit volume due to the spray, *k* is the turbulent kinetic energy (obtained by solving the transport equation, which is discussed later), and *g* is the gravitational acceleration, which is assumed to be constant.

Equation 4 presents the energy equation of the fluid domain.

$$\frac{\partial \rho I}{\partial t} + \nabla \cdot (\rho \mathbf{u} I) = -p\nabla \cdot (\mathbf{u}) - \nabla \cdot \mathbf{J} + \rho\epsilon + \dot{Q}^s + \dot{Q}^c \quad (4)$$

where I is the specific internal energy, exclusive of chemical energy. The heat flux vector, **J**, is equal to the sum of the contributions due to heat conduction and enthalpy diffusion. $\dot{Q}^s$ is the spray interaction term and $\dot{Q}^c$ is the chemical heat release term.

The Characteristic Time Scale Combustion (CTC) model has been employed to deal with the complex turbulence-chemistry interactions. This model uses the k-ε model for turbulent transport and assumes that each species' density approaches its local thermodynamic equilibrium over a characteristic time scale τ_c, which is dependent on the turbulent mixing time $\tau_t \propto k/\varepsilon$ and the chemical time scale τ_l. This model yields results that are in good agreement with measured cylinder pressure traces (Kong and Reitz 2002).

The above governing equations and submodels have been embedded in commercial software package ANSYS Forte (2017) for 3D CFD engine simulations in the present work. Forte code incorporates ground-breaking technology to allow the use of multi-component surrogate fuel models with comprehensive spray fluid dynamics without blowing up simulation turn-around time. Forte takes advantage of real fuel chemistry models for better results without the need for expert calibration. It couples a conventional chemistry solver (ODEs) with advanced chemistry solution techniques, which increase the chemistry solution efficiency with a minimal loss of accuracy. In addition, to remove the mesh-size dependency for liquid droplet-ambient gas coupling encountered in the Kelvin-Helmholtz/Rayleigh-Taylor (KH-RT) breakup model, the code uses an unsteady gas-jet model in which the axial droplet-gas relative velocity is modeled using the unsteady gas-jet theory rather than discretization on the CFD mesh. These advanced techniques make it possible to perform engine simulations using a detailed chemistry with a relatively coarse mesh while

maintaining high numerical accuracy. The submodels embedded in the Forte code are listed in Table 4; a more detailed description of the system is provided in the Forte user manual.

Table 4. The submodels employed in the ANSYS Forte software package.

Turbulence model	RNG κ-ϵ model
Breakup model	KH-RT coupled with gas-jet model
Collision model	Collision radius of influence model
Spray/wall interaction model	Naber and Reitz model
Heat transfer model	Improved law-of-the-wall
Evaporation model	Discrete multi-component
Combustion model	Detailed chemistry
Turbulence/chemistry interaction	Mixing time scale model
Soot model	Hiroyasu soot formation and Nagle/ Strickland-Constable oxidation models
NOx formation model	Thermal and prompt NO

2.3 COMBUSTION MECHANISMS

The real combustion of hydrocarbons involves hundreds of species and chemical reactions, and it is necessary to use validated detailed and reduced models to develop an accurate model. The model used in this work is based on mechanism of so-called surrogate fuel components, used to represent real fuels. In this work, the diesel oil was represented by the diesel oil surrogate (DOS) and the biodiesel by rapeseed methyl ester (RME). A summary of the main considerations of these mechanisms is shown below.

A diesel surrogate model developed for Diesel oil #2 was selected as base model in this work. This model is represented by a blend of n-heptane, C_7H_{16} (70 vol%) and toluene C_7H_8 (30 vol%) which represent aliphatic components and aromatic components. Since n-heptane has cetane

number of approximately ~56, which is similar to the cetane number of conventional Diesel oil, and toluene contributes to soot formation. Since in the surrogate model, fuel decomposition is realized in the global stage, the fuel chemical formula has to be replaced by $C_{14}H_{28}$ to meet the specified proportion between the substituent components, C_7H_{16} and C_7H_8. Therefore, an oxidizing pyrolysis process (Reaction 1 in Table 5) is used to consider the decomposition of this molecule into the components of the substitute fuel. The combustion mechanism of the diesel surrogate involves 68 species participating in 280 reactions, validated through a shock tube and in studies involving in-cylinder combustion. Empirical estimates of the forward reaction rate parameters for the irreversible global reactions of diesel surrogate model are shown in Table 5. This model and the sub-mechanisms for n-heptane and toluene oxidation have been well validated against experiments in terms of spray properties, Cetane number, autoignition delay time (Golovitchev et al. 2007; Gustavsson and Golovitchev 2003).

Table 5. Global reactions (forward reaction rate: $\boldsymbol{k_f = A_f T^{n_f} exp(-\frac{E_f}{RT})}$ in cm^3, mole, sec, cal unit, AE_f and AE_o denote concentration exponents for fuel and oxidizer, respectively.)

	Global Reaction	A	n	E	AE_f	AE_o
1	$5C_{14}H_{28} + O_2 \rightarrow 7C_7H_8 + 3C_7H_{16} + 2H_2O$	$1x10^{13}$	0	30000	0.25	1.5
2	$C_{19}H_{36}O_2 + O_2 \rightarrow MD + MB + C_3H_4$	$5x10^{11}$	0	10500	0.15	1.5
3	$MD \rightarrow C_7H_{16} + MP2D$	$8x10^{12}$	0	0	—	—

The biodiesel combustion process was represented by a biodiesel surrogate, with physical and thermal properties represented by methyl oleate ($C_{19}H_{36}O_2$). The combustion mechanism was generated by combining the combustion submechanisms of DOS, reduced mb (methyl butanoate) and md (methyl decanoate). The methyl oleate compound is one of the main compounds of the real RME fuel, and its decomposition in MD ($C_{11}H_{22}O_2$), MB ($C_5H_{10}O_2$) and allene (C_3H_4)

represents the first step of the combustion mechanism (Reaction 2 in Table 5). The MD is then decomposed into n-heptane and MP2D ($C_4H_6O_2$). The biodiesel combustion model has validated against the experimental results in terms of auto-ignition delays (Golovitchev and Yang 2009), cetane number and spray characteristics (Yang et al. 2013), e.g. spray penetrations, life-off.

The liquid properties of blended fuels were modelled using mixing rules, in the form of a virial equation of state as shown in Eq. 5, to extend the fuel library. Applying the rules involves calculating arithmetic means to obtain energy parameters (e.g. temperature) or geometric means to compute size parameters (e.g. volume) in Eq. 6.

$$Q_m = \sum_i \sum_j y_i\, y_j Q_{ij} \tag{5}$$

$$Q_m = \begin{cases} \sum_i y_i Q_i & \text{if } Q_{ij} = \dfrac{Q_{ii} + Q_{jj}}{2} \\ \left(\sum_i y_i \sqrt{Q_i}\right)^2 & \text{if } Q_{ij} = \left(Q_{ii} Q_{jj}\right)^{1/2} \end{cases} \tag{6}$$

where Q_m is the property of the blend, Q_{ii} and Q_{jj} are the properties for pure component, and y_i and y_j are the volumetric ratios of each pure component.

Therefore, for the blended fuel B8, the extracted the property data from the library for the individual components, diesel oil and biodiesel, and calculated the blend's properties according to the volumetric ratios of the components.

2.4 MECHANISM OF NO_X FORMATION

The four main mechanisms in the formation of nitrogen oxides can be summarized in: thermal mechanism, prompt mechanism, nitrous oxide (N_2O) and fuel-bond nitrogen mechanism. The thermal mechanism, proposed by Zel'dovich et al. (1947), involves a series of elementary reactions with high activation energy, due to the strength of the triple bond of the N_2 molecule. It is considered as the main mechanism in NOx formation in internal combustion engines. This

mechanism is very sensitive to the combustion temperature, which in diesel engines is determined by the properties of the liquid fuel, such as cetane number and viscosity; by the thermal-physical properties of the vapor, such as enthalpy and head capacity; and by the rate of heat loss, which is primarily due to the radiation of the soot particles. The radical O may be derived from O_2 or from oxygenated fuel molecules (Yang et al. 2012).

In this work, the Zeldovich mechanism is one of the main factors for the determination of NOx emissions. The N_2O mechanism has a minor role in the overall generally formation of NO, being typically considered as part of the thermal mechanism, whose combination is considered as the thermal NO/N_2O route. The main step of the N_2O mechanism also involves an O atom attacking N_2 in the presence of a third component to form N2O, which can subsequently react with O to produce NO. In the prompt mechanism, the main characteristic is that the CH radical (methylidyne), which is formed exclusively in the flame front, reacts with the nitrogen of the air to form the hydrocyanic acid (HCN), which then reacts to form NO. The NCN pathway (Konnov 2009) of prompt NO formation, which involves 27 reactions, has been implemented in the main combustion kinetics together with the thermal NO/N_2O mechanism. Since the fuels studied have minimal amounts of nitrogen, NO formation by the fuel-bond nitrogen mechanism was not considered in the present work.

2.5 NUMERICAL MODEL

The engine numerical model was constructed for a study focused on understanding the impact of the use of exhaust gas recirculation on NOx emissions. The three-dimensional model of the engine combustion chamber was built in 360°. The diesel oil injector was positioned according to the experimental measurements. A schematic diagram illustrating two-dimensional piston bowl profile is presented in Figure 2. The piston bowl offset 5.5 mm from the piston center. A full

Journal of Engineering for Gas Turbines and Power. Received March 27, 2021;
Accepted manuscript posted July 29, 2021. doi:10.1115/1.4051951

surface mesh of piston bowl and the position of the injector used to model the MWM 229/4 diesel engine is shown in the left of Figure 2. The numerical grid was built by ANSYS Forte. A study on the effects of the numerical grid size on the results was carried out, seeking to verify the independence of solution in relation to the refinement of the numerical grid. The adaptive refinement technique was used to achieve a better numerical solution in the regions near the walls, where the remapping of the numerical mesh is determined according to the temperature and velocity gradient (Battistoni et al. 2015; Divekar et al. 2016). The final numerical grid was chosen according to the comparison with the experimental results and by the variation between the numerical results. There was a tendency of reduction of the pressure inside the cylinder with a greater refinement of the mesh, until stabilization of the results was identified, as also verified by Wei et al. (2014). The mesh used to present the results has about 440,000 elements at the beginning of the closed engine cycle, at 150 °CA Before TDC (BTDC), and 41,000 at the TDC. The time step of the solution was on average $1x10^{-5}$ s. The processing time was about 22 hours on a computer with Windows® 10 64-bit operating system, Intel® Core ™ i7-4790S processor, 8 cores, 16 GB RAM and 3.2 GHz clock.

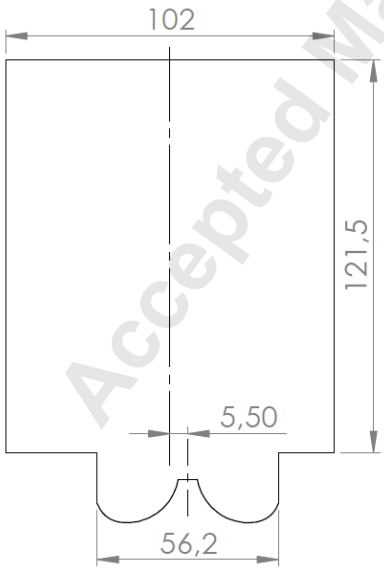

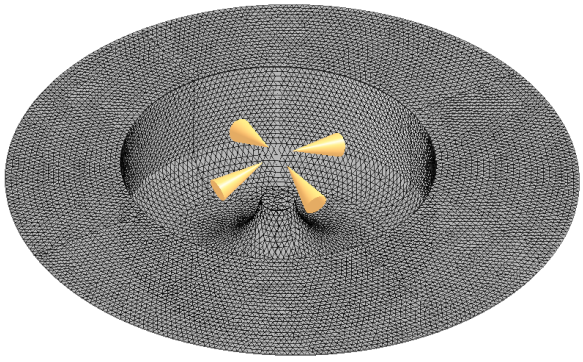

Figure 2. A schematic diagram (dimension in mm) illustrating 2-dimensional piston bowl profile and a full surface mesh of piston bowl and the position of the injector used to model the MWM 229/4 diesel engine.

The closed cycle of combustion was simulated, that is, between 150°CA BTDC and 150°CA After TDC (ATDC). Recirculation of the exhaust gases was considered by the inclusion of CO_2 and H_2O, the main components of the exhaust gases, in the initial composition of the air inside the cylinder. The possible water condensation due to the cooling system was not measured experimentally and thus was not considered in the numerical modelling. The operating conditions and 10% EGR compositions used for the engine simulations are presented in Table 6.

Table 6. Operating conditions of the engine simulation.

Parameter	**B8**	**B8 + EGR**
Nominal load (kW)	30	30
Engine speed (rpm)	1800	1800
Injector nozzle diameter (mm)	0.3	0.3
Included angle of spray (°)	151	151
Spray cone ½ angle (°)	12.5	12.5
Injected mass/stroke (B8)	35	36
Fuel temperature (K)	350	350
Start of injection (°CA BTDC)	20	20
Injection duration (°CA)	23	23
Walls temperature (°C)	~450	~450
Air initial composition	21% O_2	20.79% O_2
(indicates 0% (left) and	79% N_2	76.77% N_2
10% (right) EGR levels)		1.73% CO_2

		0.71% H_2O
Initial pressure (kPa)	95	93
Initial temperature (K)	400	410

The injection profile (also called "rate shape") is a crucial parameter for accurate CFD predictions. Ideally, a rate of injection on injection pressure profile should be measured for the current injector to improve the fidelity of CFD model. Due to the lack of this information, an injection rate profile published in (Singh et al. 2006) for a similar type of injector was adopted for the present study. The other parameters related to the numerical models, such as turbulence model and chemical kinetics, were maintained with standard values, as recommended by the ANSYS Forte Theory Manual. ANSYS Forte uses advanced control to adapt the convergence criteria according to the gradients found in the solution variables, guaranteeing the accuracy of the results.

3. RESULTS AND DISCUSSION

3.1 Numerical Validation

The in-cylinder pressure and rate of heat release (RoHR) as functions of crank angle for MWM 229/4 diesel engine fueled by B8 with 0% and 10% EGR levels at the load of 30 kW were predicted and compared with experimental data, shown in Figure 3. Experimental data sampled for 300 consecutive combustion cycles are also plotted for the purpose of validation.

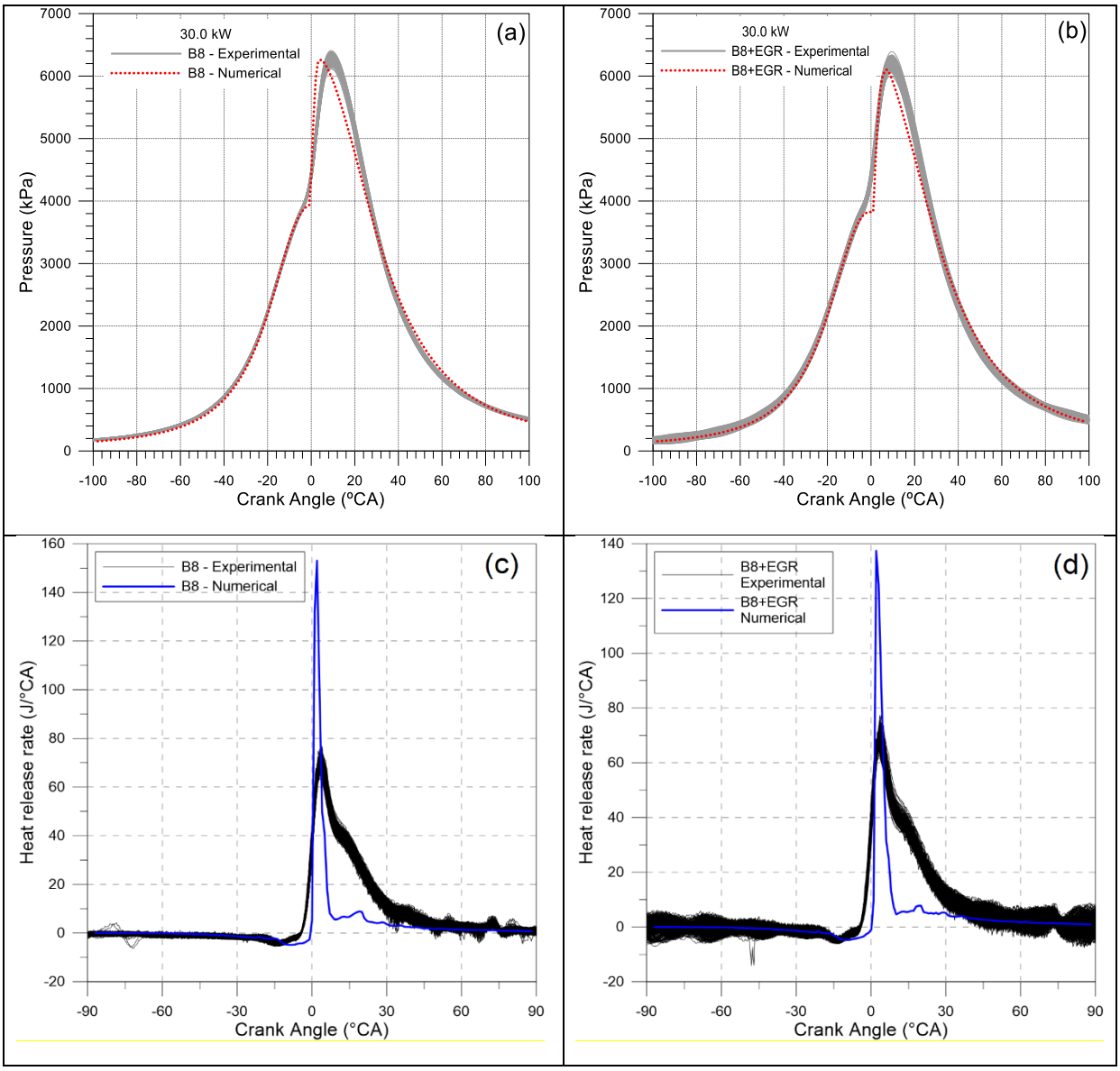

Figure 3. Comparison of measured and predicted in-cylinder pressures a)&b), and rate of heat release c)&d) for MWM 229/4 diesel engine fueled by B8 with 0% and 10% EGR levels at the load of 30 kW. The experimental data was sampled for 300 consecutive combustion cycles.

The predicted peak pressures are slightly 0.5-1 % lower than the experimental mean value for both with and without EGR cases. In addition, numerical pressure peaks take place of 2~5 Crank Angle Degrees (CADs) ahead of the experimental value. The predicted RoHR starts to increase ~ 5 CADs later than the measured data, probably because the combustion model is highly sensitive

to the cooling effect of the large quantity of injected fuel. RoHR was predicted to be higher than the measured values during the early combustion phase. At higher CAD values, the predicted curves become lower than that for the experimental data. This means that the current B8 surrogate fuel model burns more rapidly than the real fuel and has a shorter combustion phase. Both numerical and experimental RoHR curves has shown that the impact of mild EGR on delaying the start of combustion is minimal. To obtain a closer approximation between the results, a specific chemical model must be developed for the real diesel and biodiesel mixtures.

In-cylinder pollutant concentrations (NO and NOx) are plotted with respect to the crank angle, presented in Figure 4. The engine-out emissions were also measured and presented with error bar. The numerical values of case B8 are within the ranges of experimental uncertainties. For the B8 + EGR case, the numerical value of NOx is also within the range of experimental uncertainties, but the numerical value of NO emissions is 10% lower than the mean experimental value and 5% lower than the lower limit of experimental uncertainty. These differences are associated with the displacement of the pressure curve (i.e. ~1% lower in peak pressure), that slightly alters the NOx formation condition (i.e. in-cylinder temperature). According to the results, it was considered that the numerical study showed good agreement with the experimental results, assuming, then, that the numerical behaviour of the gases inside the cylinder approaches the actual behaviour. Meanwhile, the results show that the NOx formed mechanism (combined thermal route and prompt route) adopted in the present work is capable to accurately predict NOx emissions from the diesel engine.

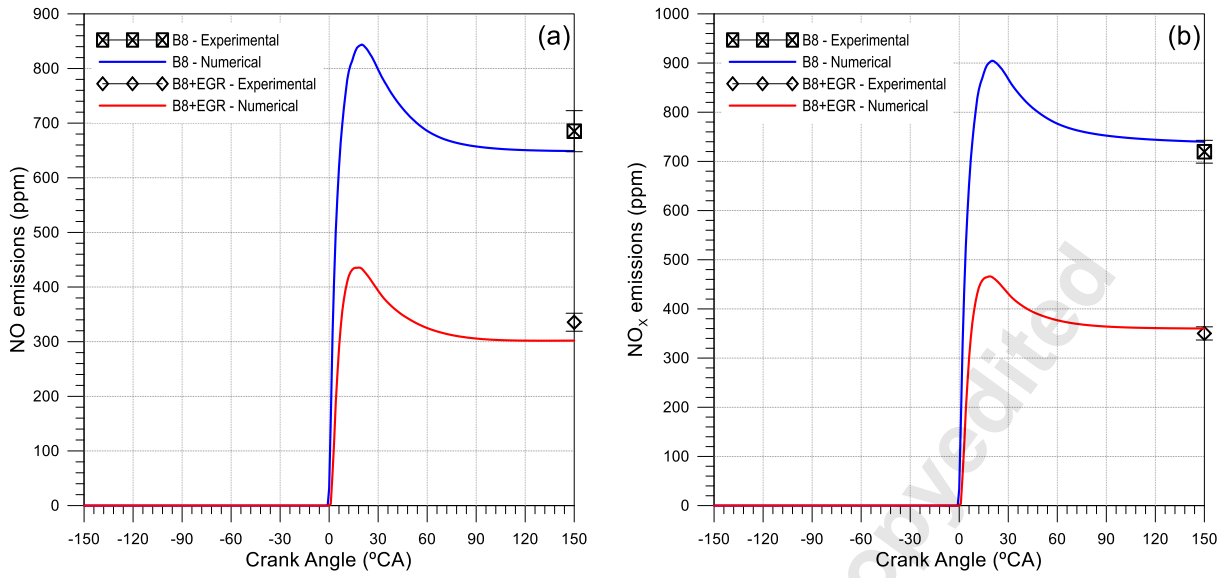

Figure 4. Comparison of measured and predicted a) NO, b) NOx species concentration from MWM 229/4 diesel engine fueled by B8 with 0% and 10% EGR levels at the load of 30 kW

3.2 Experimental and Numerical Results

The experimental engine brake specific fuel consumption (BSFC) for the different operating conditions are shown in Figure 5. There is a trend of increasing the BSFC when using EGR for higher loads. Several factors can increase the fuel consumption when using the EGR technique, including the deterioration of combustion quality, by reducing the air/fuel ratio and the oxygen availability, and the longer ignition delay (Divekar et al. 2016). These factors also reduced the brake thermal efficiency. The reduction of EGR temperature (EGR cooling) can mitigate the prejudicial EGR factors (Hountalas et al. 2008).

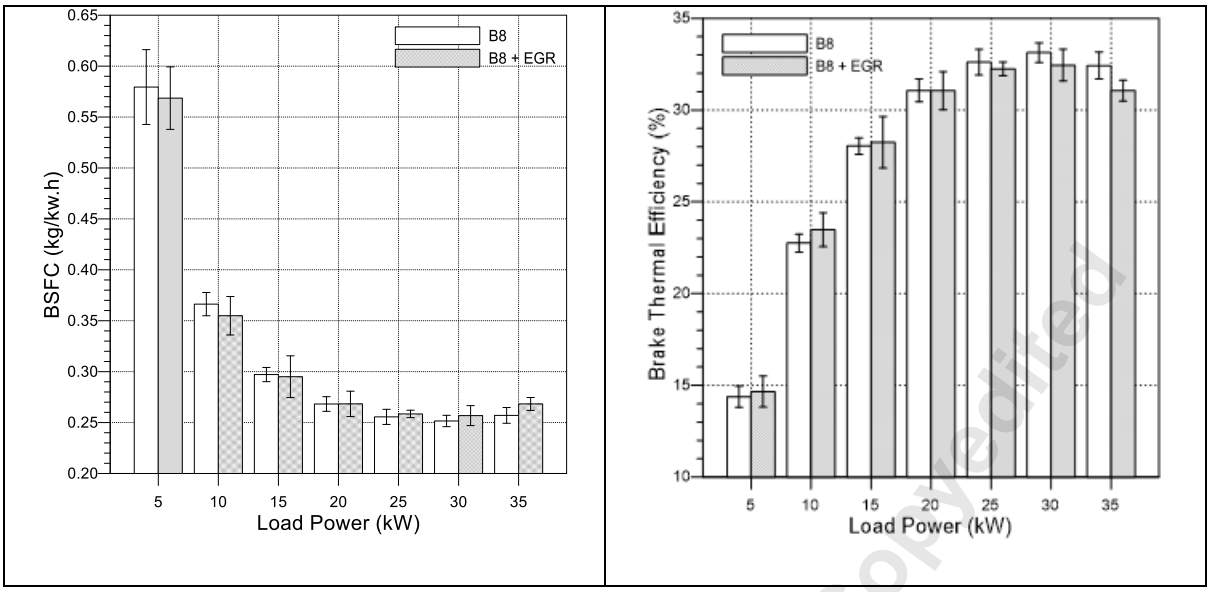

Figure 5. Brake Specific fuel consumption, BSFC, and brake thermal efficiency for MWM 229/4 diesel engine fueled by B8 with 0% and 10% EGR levels under different loads.

The EGR leads to a slight reduction of the in-cylinder pressure during the compression stroke and this reduction becomes noticeable during the combustion phasing and expansion stroke. Broadly speaking, three classes of explanation have been put forward: the increase of specific heat of the air-fuel mixture with the presence of the exhaust gases, the reduced O_2 availability which has a negative effect on the combustion rate, the dissociation of CO_2 and H_2O species. The combination of these factors cause a cooling effect, and thus the reduction of in-cylinder pressure and heat release rate. This cooling effect becomes noticeable at higher loads as shown in Figure 6.

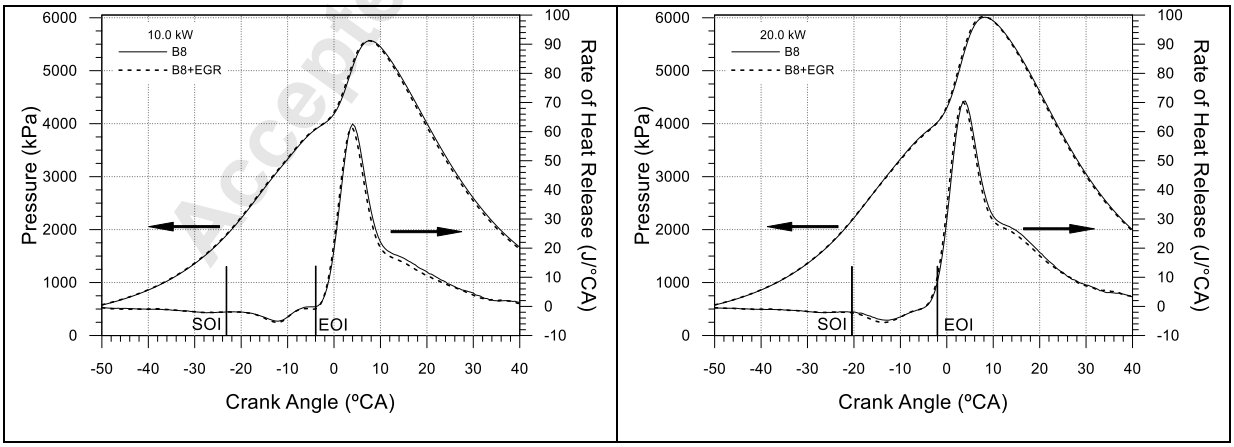

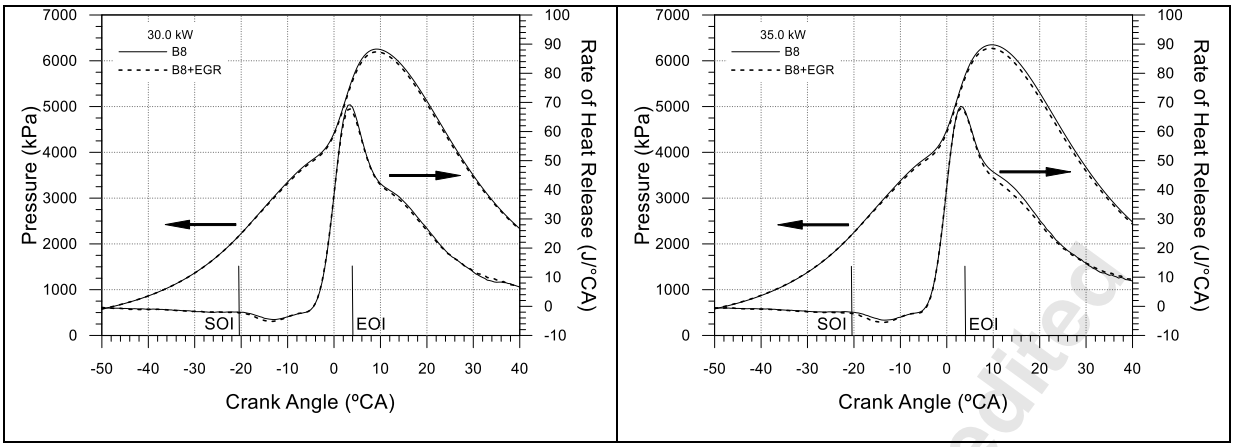

Figure 6. The history of in-cylinder pressure and rate of heat release rate for diesel engine fueled by B8 with 0% and 10% EGR levels under different loads. Start of Injection, SOI, and End of Injection, EOI label the fuel injection period.

The emission concentrations (CO_2, CO, O_2 and THC) in exhaust under different engine operating conditions are shown in Figure 7. As can be seen, all species concentrations decrease as engine load increases from 5 kW and remain constant 30 kW, except CO which reaches the lowest level at 25 kW, then climbs up a little bit at higher loads. In addition, the results suggest that the CO_2 and CO emission increase with the use of mild EGR. While, the excess oxygen, O_2, and Total Hydrocarbon, THC decrease. The increase of CO_2 emissions is mainly due to the intake replenishment (Zheng et al. 2004) in which fresh air containing negligible amount of CO_2 is replenished by the recycled portion that carries a substantial amount of CO_2 varying between 4% and 12%. These increases are within the uncertainties range (indicated by error bar on each column) for most engine loads except the lowest load, 5 kW in Figure 7a). Regarding the CO emissions, adding exhaust gas to the air-fuel mixture reduces the oxygen availability, slows the combustion reaction rates, and reduces the in-cylinder temperature, which cause incomplete combustion (Zheng et al. 2004) and more CO emissions. As expected, excessive oxygen has been detected in the exhaust, which indicates diesel engine operates under the lean condition. Figure

Journal of Engineering for Gas Turbines and Power. Received March 27, 2021;
Accepted manuscript posted July 29, 2021. doi:10.1115/1.4051951

7c) shows that the amount of excessive oxygen decreases as engine load increases for both 0% and 10% EGR levels. The mild EGR reduces the excessive oxygen by 17% (at 5 kW) and 36% (at 35 kW) compared to 0% EGR case, which evidences the reduction of oxygen availability in the intake manifold. The reduction of total unburned hydrocarbons, i.e. THC, by mild EGR is presented in Figure 7d). This reduction could be associated with the reburning of the hydrocarbons that returns to the combustion chamber by the exhaust gas recirculation (Agarwal et al. 2011).

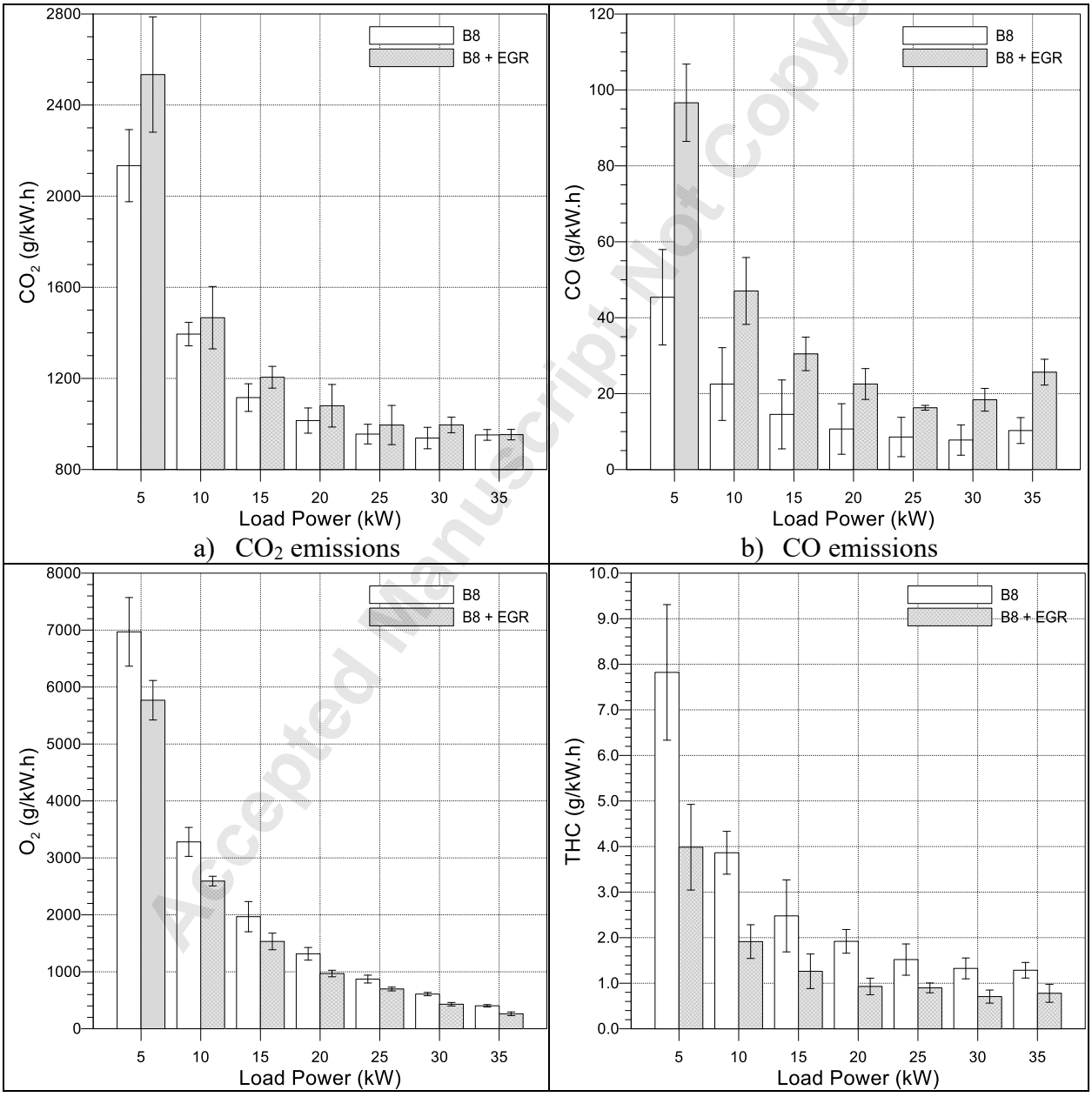

c) O_2 emissions	d) THC emissions

Figure 7. Measured exhaust emissions from MWM 229/4 diesel engine fueled by B8 with 0% and 10% EGR levels under different loads: a) CO_2, b) CO, c) O_2 and d) THC.

The effect of mild EGR on NO and NOx emissions are shown in Figure 8. Maximum reduction of 59% and 56% at the load of 35 kW have been observed for NO and NOx, respectively. It is well-known that EGR has a significant cooling effect for diesel engine combustion that reduces the combustion temperature and thus the thermal formation of NO and NOx. To obtain a new insight into the impact of EGR on NOx emission from biodiesel engine, 3D CFD engine modelling under the load of 30 kW has been conducted and the numerical results have been analyzed and discussed hereinafter.

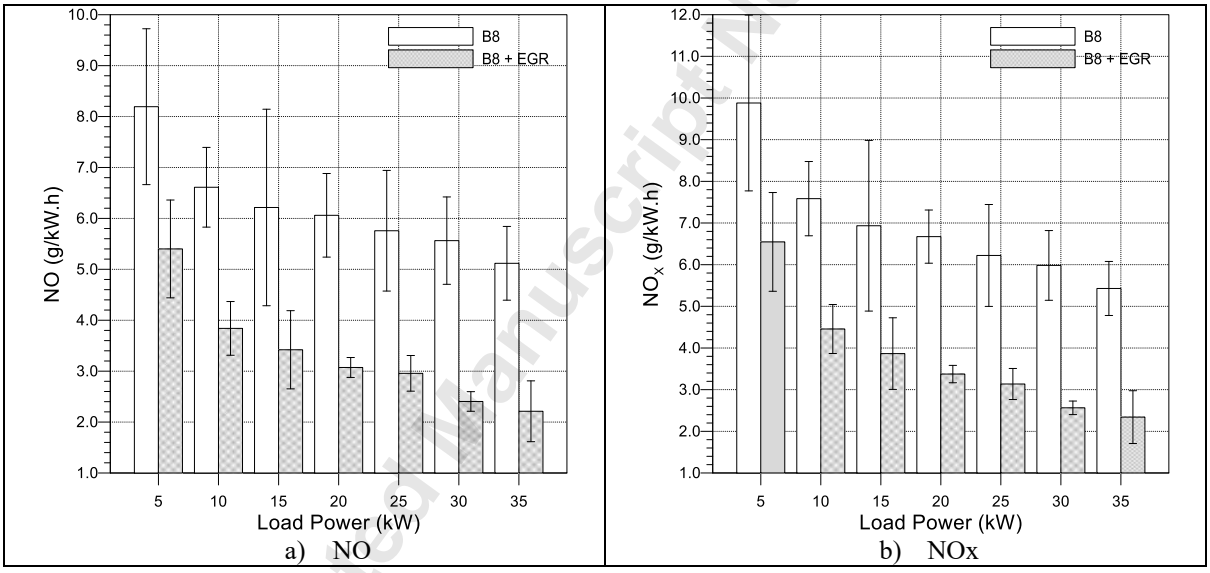

Figure 8. Measured a) NO, b) NOx emissions for MWM 229/4 diesel engine fueled by B8 with 0% and 10% EGR levels under different loads.

The temperature distribution and the fuel spray at TDC for the case B8 at 30kW load are shown in Figure 9. As can be seen, the fuel spray is directed towards the cylinder wall and distributed within the combustion chamber when it impinges the piston bowl surface. The cylinder walls meet around 900K, while the cold fuel, around 400K, causes cooling of the stricken region.

Journal of Engineering for Gas Turbines and Power. Received March 27, 2021;
Accepted manuscript posted July 29, 2021. doi:10.1115/1.4051951

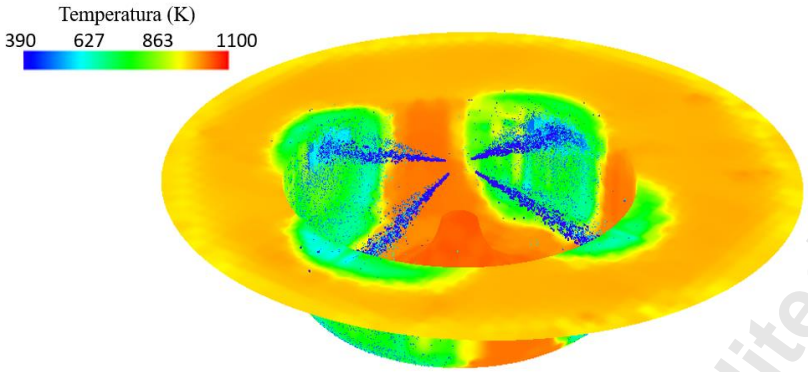

Figure 9. Temperature distribution of cylinder and diesel oil spray at TDC in case B8 for the load of 30 kW.

The NO/NOx concentration in the cylinder for the load of 30 kW as a function of the crank angle (see Figure 4) shows that, in both cases, the NO/NOx concentration increases rapidly after the start of combustion and that the majority of the NO/NOx are formed during the early combustion phase (< CA25). The combustion temperature during the late expansion stroke does not affect the final NO concentration.

The contours shown in Figure 10 illustrate the equivalence ratio, ϕ, cylinder temperature and NO mass fraction at different CADs for the engine in B8 mode. It is observed that the rich air-fuel mixture (ϕ >1) is formed near the walls of the combustion chamber and the region of the injector. NO emissions are formed in high-temperature and O_2-rich local regions where the combustion temperature is above 2300 K. NO starts to form ATDC and the region of high NO concentration appears around the periphery of the reaction mixture. There is a high NO concentration in the region near the injector, which spreads along the cylinder due to the movement of the air.

Position (ATDC)	**Fuel/air equivalence ratio ϕ**	**Temperature (K)**	**NO (mass fraction)**

Journal of Engineering for Gas Turbines and Power. Received March 27, 2021;
Accepted manuscript posted July 29, 2021. doi:10.1115/1.4051951

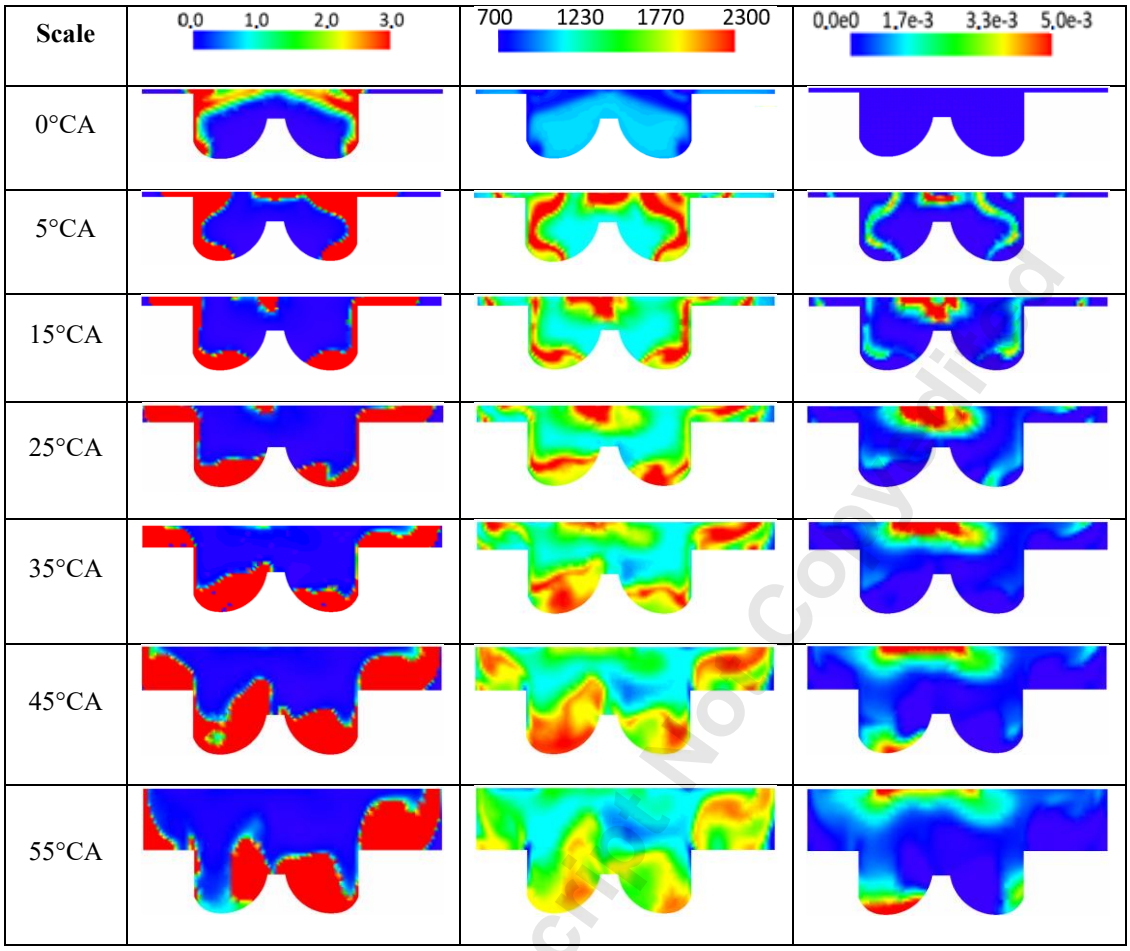

Figure 10. Contours of the equivalence ratio of the fuel/air mixture, temperature in the cylinder and mass fraction of NO for MWM 229/4 diesel engine fueled by B8 without EGR at the load of 30 kW.

The central region of the combustion chamber presents lower temperatures and, consequently, lower concentration of NO. There is marginal NO formed throughout the spray, since the start of combustion occurs at the end of the fuel injection. The results indicate, therefore, that a large part of the NO is formed in regions of high temperature, that is, by the thermal mechanism. The eccentricity of the combustion chamber of the cylinder causes asymmetry in the temperature distribution, especially during the expansion process. This is probably due to the asymmetric air movement in the squish volume. The left part of squish volume is smaller than the right part, which

allows air to move downwards rather than transversely occurred at the right part. This downward flow motion enhances the air-fuel mixing in the piston bowl, and favors the combustion process.

The impact of mild EGR on fuel/air equivalence ratio, temperature and mass fraction of NO is illustrated by contour maps shown in Figures 11&12. The results indicated a reduction of in-cylinder local temperature when it is at TDC, associated to the increase of the heat capacity of the mixture, with the recirculation of CO_2. There is also a wider range of cylinder rich mixture with exhaust gas recirculation due to the reduction of the O_2 concentration in the air-fuel mixture.

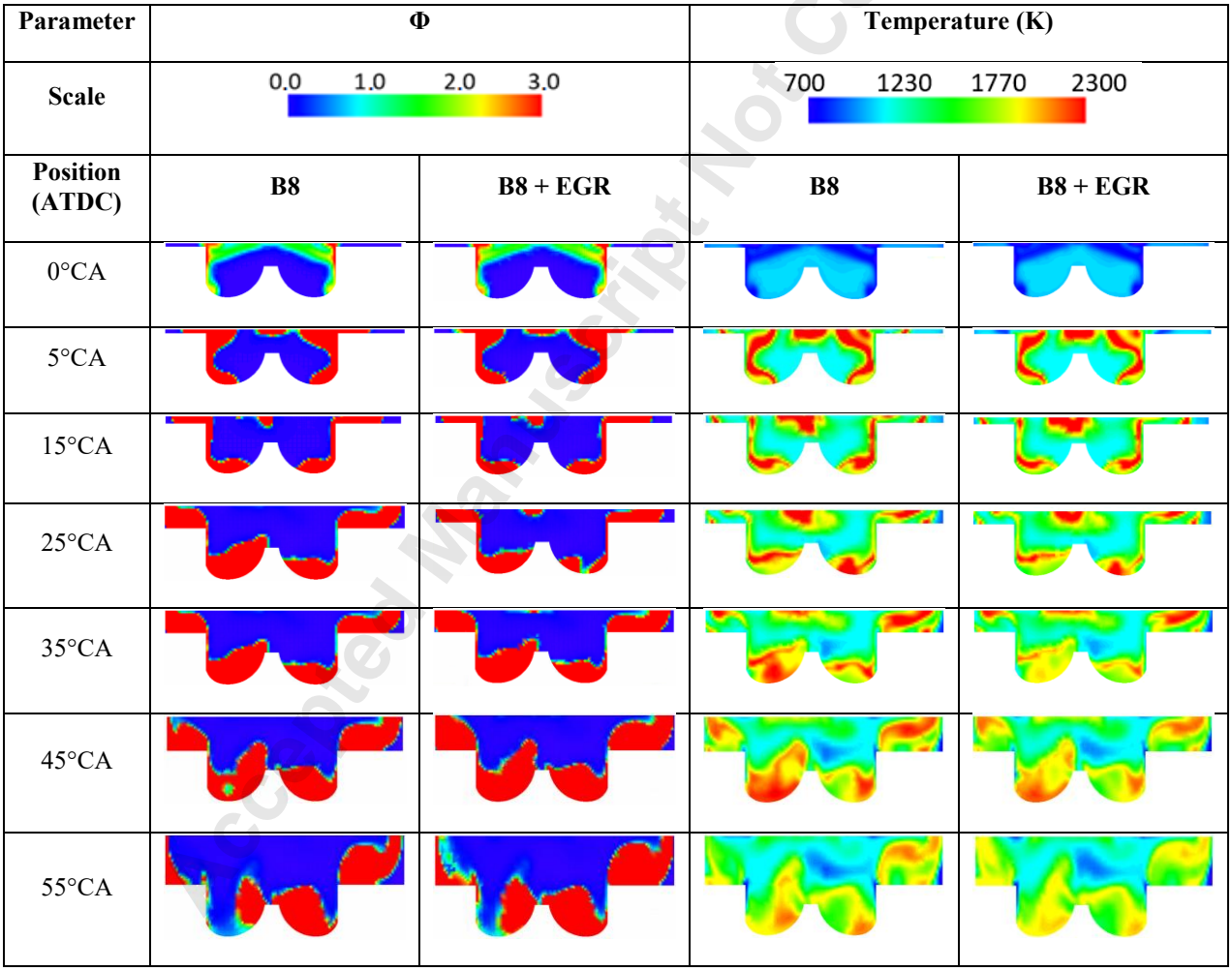

Figure 11. Contours of the equivalence ratio of the fuel/air mixture and temperature for MWM 229/4 diesel engine fueled by B8 with and without EGR under the load of 30 kW.

Journal of Engineering for Gas Turbines and Power. Received March 27, 2021;
Accepted manuscript posted July 29, 2021. doi:10.1115/1.4051951

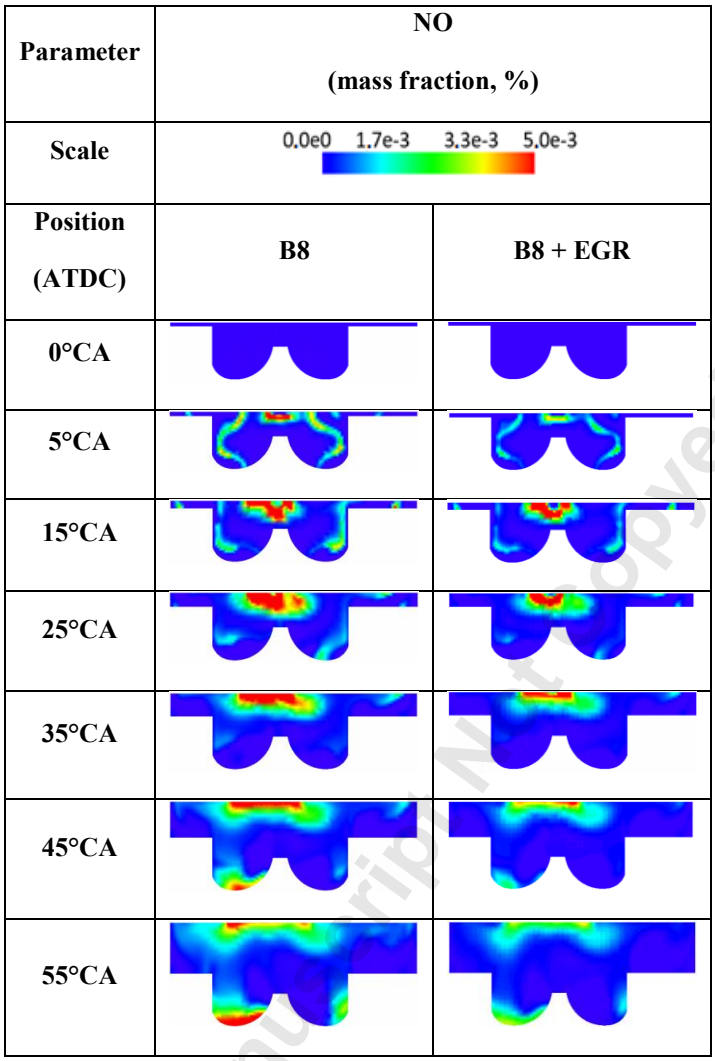

Figure 12. Contour of the NO emission distribution for MWM 229/4 diesel engine fueled by B8 with and without EGR under the load of 30 kW.

The formation of NO is clearly lower in the case B8 + EGR, since the main factors that dominate the formation of this component have been reduced, that is, temperature and O_2 concentration. NO formation is very sensitivity to temperature and equivalence ratio. A minor change in temperature and equivalence ratio may result in a notable variation of NO concentration. It is observed that the region of higher NO formation in the case B8 + EGR is in the upper face of the combustion chamber, where higher temperatures occurred in an environment of poorer mixtures. The reduction

in in-cylinder temperature also justify the CO emissions increases using EGR, indicated by the experimental results in Figure 8.

The history of averaged in-cylinder temperature and fuel/air equivalence ratio are plotted in Figure 13. The curves showed that the averaged in-cylinder temperature reduced when using EGR, but not as much as showed in the local temperature results, which is one of the main factors in NOx formation. The temperature difference between B8 and B8+EGR is relatively modest and so cannot be responsible for the large (<50%) decrease in NOx emissions. The mean equivalence ratio increased by a large amount (around 30%), when using EGR, indicating that is the main factor in NOx reduction. This result demonstrates that NO formation is not governed by thermal factors alone. An increase in local equivalence ratio and decrease in local temperature of in-cylinder combustion makes the combustion path pass through lower NOx zone in the ϕ-T diagram, see Figure 14. The comparative study of diesel and biodiesel combustion under equilibrium conditions indicates that slightly lean mixtures favour NO level (Yang et al. 2012) according to the NO-ϕ correlation curve. On the contrary, the comparatively rich combustion inhibits the NO formation for B8+EGR case.

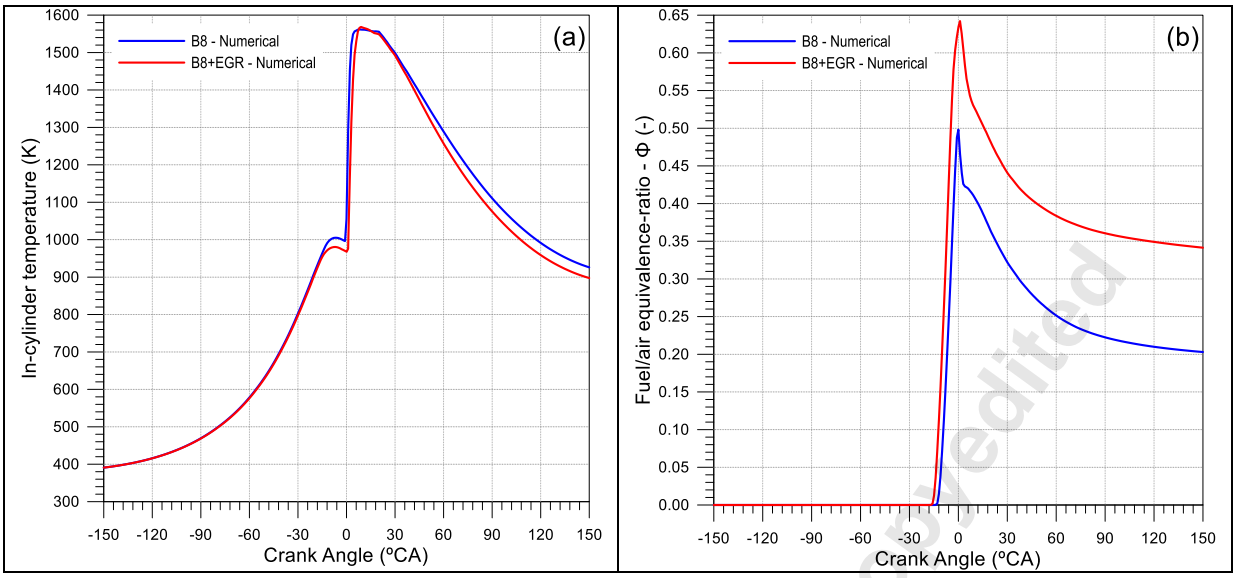

Figure 13. Predicted mean in-cylinder a) temperature, b) equivalence ratio of the fuel/air mixture for MWM 229/4 diesel engine fueled by B8 with 0% and 10% EGR levels at the load of 30 kW.

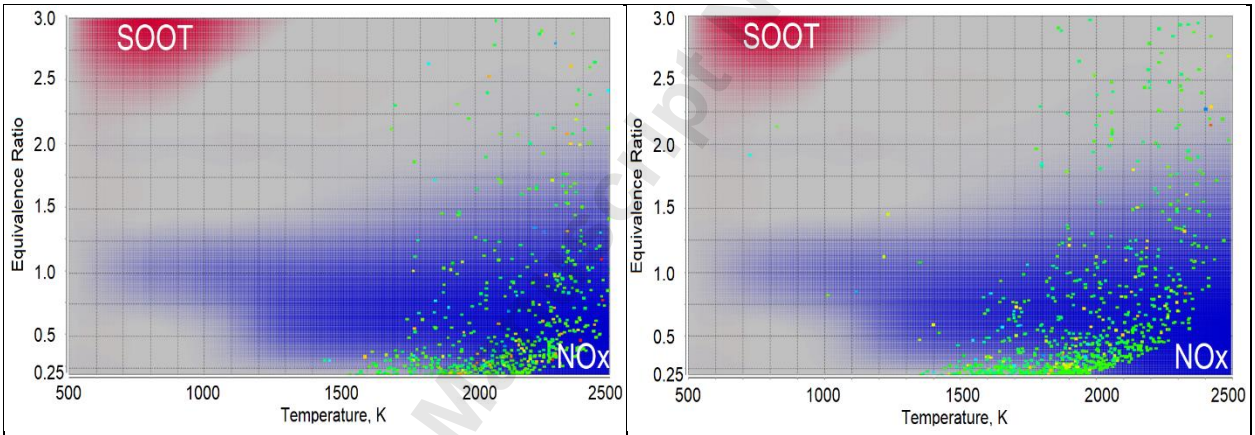

Figure 14. Parametric ϕ-T emission maps for instantaneous (at 25 CAD ATDC) soot and NOx concentrations in the MWM 229/4 diesel engine fueled by B8 with a) 0% and b) 10% EGR at the load of 30 kW. The cluster points representing in-cylinder conditions (vapor mass, temperature and equivalence ratio).

4. CONCLUSIONS

This study showed the effects of using cold EGR in a diesel power generator fuelled by B8. The recirculation of 10% of the exhaust gas slightly affected the engine specific fuel consumption and

fuel conversion efficiency and proved to be effective in reduce the NOx emissions, reaching a reduction of up to 56%. However, the use of 10% EGR increased CO and CO_2 emissions, due to the incomplete combustion caused by the lower availability of oxygen. This undesirable NO-CO trade off seems unavoidable in the present diesel engine. Therefore, the optimum emissions and engine performance should be determined for the optimum EGR rate, to obtain an acceptable engine performance and meet emissions regulations.

The numerical study showed that the NO formation in the engine is mainly due to the thermal mechanism. Whereas a new perspective from the ϕ-T emission map analysis is that the mild EGR alters the local equivalence ratio of air-B8 mixtures in the diesel engine. The use of 10% EGR inhibits the NO formation by a little reduction of the local in-cylinder temperature and, mainly, by creating comparatively rich combustion. Thus, the balance of importance between EGR and equivalence ratio becomes essential in diesel engine fuelled by biodiesel. The EGR use reduced THC emissions up to 52%. In contrast, CO_2 and CO emissions increased when using EGR, up to 19% and 155%, respectively.

ASSOCIATED CONTENT

Supporting Information

The following files are available free of charge.

Appendix A Measurement device specifications.docx

AUTHOR INFORMATION

Corresponding Authors

*Junfeng Yang J.Yang@leeds.ac.uk

ACKNOWLEDGMENT

The authors thank CAPES, CNPq, and FAPEMIG for the financial support for this work.

REFERENCES

Agarwal, D., Singh, S.K., Agarwal, A.K. (2011). Effect of Exhaust Gas Recirculation (EGR) on performance, emissions, deposits and durability of a constant speed compression ignition engine. *Appl. Energy*. 88, 2900–2807.

Andreae, M., Fang, H., Bhandary, K. (2007). Biodiesel and Fuel Dilution of Engine Oil, SAE Technical Paper 2007-01-4036, doi:10.4271/2007-01-4036.

Brazil's National Agency of Petroleum, Natural Gas and Biofuels (2014). ANP Resolution No.45/2014.

ANSYS., (2017). FORTE Theory Manual, Release 18.1, ANSYS, Inc

Asad, U., Kumar, R., Zheng, M., Tjong, J. (2015). Ethanol-fueled low temperature combustion: A pathway to clean and efficient diesel engine cycles. *Appl. Energy*. 157, 838–850.

Balamurugan, T., Arun, A., Sathishkumar, G.B. (2018). Biodiesel derived from corn oil – A fuel substitute for diesel. *Renew Sustain Energy Rev*. 94, 772–778.

Battistoni, M., Mariani, F., Risi, F., Poggiani, C. (2015). Combustion CFD modeling of a spark ignited optical access engine fueled with gasoline and ethanol. *Energy Procedia*. 82, 424-431.

Boccardi, S., Catapano, F., Costa, M., Sementa, P., Sorge, U., Vaglieco, B.M. (2016). Optimization of a GDI engine operation in the absence of knocking through numerical 1D and 3D modeling. *Adv. Eng. Softw*. 95, 38-55.

Bozza, F., De Bellis, V., Teodosio, L. (2016). Potentials of cooled EGR and water injection for knock resistance and fuel consumption improvements of gasoline engines. *Appl. Energy*. 169, 112–125.

Brazil. Law Nr. 13033., (2016). http://www.planalto.gov.br/ccivil_03/_ato2015-2018/2016/lei/L13263.htm.

Cameretti, M.C., Tuccillo, R., Simio, L. De., Iannaccone, S., Ciaravola, U. (2016). A numerical and experimental study of dual fuel diesel engine for different injection timings. *Appl. Therm. Eng*. 101, 630-638.

Çelik M. (2017). Examining combustion and emission characteristics of cotton methyl ester to which manganese additive material was added. *Journal of Mechanical Science and Technology*. 31(12), 6041-6050.

Çelik M., Özgören Y.Ö. (2017). The determination of effects of soybean and hazelnut methyl ester addition to the diesel fuel on the engine performance and exhaust emissions. *Applied Thermal Engineering*. 124, 124–135.

Das, S.K., Lim, O.T. (2017). Spray Simulation of n-heptane in a Constant Volume Combustion Chamber over a Wide Range of Ambient Gas Density and Fuel Temperature. *Energy Procedia*. 105, 1813-1820.

Divekar, P.S., Chen, X., Tjong, J., Zheng, M. (2016) Energy efficiency impact of EGR on organizing clean combustion in diesel engines. *Energy Convers Manag*. 112, 369–81.

Dong, S., Cheng, X., Ou, B., Liu, T., Wang, Z. (2016). Experimental and numerical investigations on the cyclic variability of an ethanol/diesel dual-fuel engine. *Fuel*. 186, 665–673.

Edara, G., Murthy, Y.V.V., Srinivas, P., Nayar, J., Ramesh, M. (2018). Effect of cooled EGR on modified light duty diesel engine for combustion, performance and emissions under high pressure split injection strategies. *Case Stud Therm Eng*. 12, 188–202.

Fraioli, V., Mancaruso, E., Migliaccio, M., Vaglieco, B.M. (2014). Ethanol effect as premixed fuel in dual-fuel CI engines: Experimental and numerical investigations. *Appl. Energy*. 119, 394-404.

Giakoumis E.G., Sarakatsanis, C.K. (2019). A Comparative Assessment of Biodiesel Cetane Number Predictive Correlations Based on Fatty Acid Composition. *Energies*. 12(422),1-30.

Graboski, M.S., McCormick, R.L. (1998). Combustion of fat and vegetable oil derived fuels in diesel engines. *Prog Energy Combust Sci.* 24, 125–164.

Golovitchev, V.I., Montorsi, L. and Denbratt, I. (2007). Numerical Evaluation of a New Strategy of Emissions Reduction by Urea Direct Injection for Heavy Duty Diesel Engines. *Engineering Applications of Computational Fluid Mechanics*. 1(3):189-206.

Golovitchev, V.I., Yang, J. (2009). Construction of combustion models for rapeseed methyl ester bio-diesel fuel for internal combustion engine applications. *Biotechnol Adv*. 27, 641–655.

Gustavsson, J. and Golovitchev, V.I. (2003). Spray Combustion Simulation Based on Detailed Chemistry Approach for Diesel Fuel Surrogate Model. *SAE paper 2003-01-1848*.

Hosseinzadeh-Bandbafha, H., Tabatabaei, M., Aghbashlo, M., Khanali, M., Demirbas, A. (2018). A comprehensive review on the environmental impacts of diesel/biodiesel additives. *Energy Convers Manag*. 174, 579–614.

Hountalas, D.T., Mavropoulos, G.C., Binder, K.B. (2008). Effect of exhaust gas recirculation (EGR) temperature for various EGR rates on heavy duty DI diesel engine performance and emissions. *Energy*. 33, 272–283.

Huang, Y., Hong, G., Huang, R. (2015). Numerical investigation to the dual-fuel spray combustion process in an ethanol direct injection plus gasoline port injection (EDI + GPI) engine. *Energy Convers. Manag*. 92, 275–286.

Huang, M., Gowdagiri, S., Cesari, X.M., Oehlschlaeger, M.A. (2016). Diesel engine CFD simulations: Influence of fuel variability on ignition delay. *Fuel*. 181, 170-177.

Jothithirumal, B., Jamesgunasekaran, E. (2012). Combined impact of biodiesel and exhaust gas recirculation on NOx emissions in DI diesel engines. *Procedia Engineering*. 38, 1457-1466.

Knothe, G., Krahl, J., Van Gerpen J. (2005). *The Biodiesel Handbook*. AOCS Press, doi:10.1201/9781439822357.

Knothe, G. (2008). "Designer" biodiesel: Optimizing fatty ester composition to improve fuel properties. *Energy&Fuels*. 22, 1358-1364.

Kong, S.C. and Reitz, R.D. (2002). Application of Detailed Chemistry and CFD for Predicting Direct Injection HCCI Engine Combustion and Emissions. Proc. Combust. Inst. 29, 663–669.

Konnov, A.A. (2009). Implementation of the NCN pathway of prompt-NO formation in the detailed reaction mechanism. *Combust. Flame*. 156, 2093-2105.

Kumar, J.T.S., Sharma, T.K., Murthy, K.M., Rao, G.A.P. (2017). Effect of reformed EGR on the performance and emissions of a diesel engine: A numerical study. *Alexandria Eng. J*. 57, 517-525.

Lapuerta, M., Armas, O., Rodríguez-Fernández, J. (2008). Effect of biodiesel fuels on diesel engine emissions. *Prog Energy Combust Sci*. 34, 198-223.

Ladommatos, N., Abdelhalim, S.M., Zhao, H., Hu, Z. (1997). The Dilution, Chemical, and Thermal Effects of Exhaust Gas Recirculation on Diesel Engine Emissions - Part 4 : Effects of Carbon Dioxide and Water Vapour. *Journal of Engines*. 106, 1844-1862.

Mardi, K.M., Khalilarya, S., Nemati, A. (2014). A numerical investigation on the influence of EGR in a supercharged SI engine fueled with gasoline and alternative fuels. *Energy Convers. Manag*. 83, 260-269.

Muncrief, R.L., Rooks, C.W., Cruz, M., Harold, M.P. (2008). Combining biodiesel and exhaust gas recirculation for reduction in NOx and particulate emissions. Energy & Fuels. 22(2), 1285-1296.

Naik, C.V., Puduppakkam, K., Meeks, E. (2013). Simulation and Analysis of In-Cylinder Soot Formation in a Low Temperature Combustion Diesel Engine Using a Detailed Reaction Mechanism. *SAE Int J Engines*. 6(2), 1190-1201.

Oliveira, A., Morais, A.M., Valente, O.S., Sodre, J.R. (2017). Combustion, performance and emissions of a diesel power generator with direct injection of B7 and port injection of ethanol. *J Brazilian Soc Mech Sci Eng*. 39, 1087–1096.

Palash, S.M., Masjuki, H.H., Kalam, M.A., Masum, B.M., Sanjid, A., Abedin, M.J. (2013). State of the art of NOx mitigation technologies and their effect on the performance and emission characteristics of biodiesel-fueled Compression Ignition engines. *Energy Convers Manag*. 76, 400–420.

Puduppakkam, K.V., Liang, L., Shelburn, A., Naik, C.V., Meeks, E., Bunting, B. (2010). Predicting Emissions Using CFD Simulations of an E30 Gasoline Surrogate in an HCCI Engine with Detailed Chemical Kinetics. *SAE Technical Paper 2010-01-0362*.

Shin, B., Cho, Y., Han, D., Song, S., Chun, K.M. (2011). Hydrogen effects on NOx emissions and brake thermal efficiency in a diesel engine under low-temperature and heavy-EGR conditions. *Int J Hydrogen Energy*. 36, 6281–6291.

Singh, S., Reitz, R., Musculus, M. (2016). Comparison of the Characteristic Time (CTC), Representative Interactive Flamelet (RIF), and Direct Integration with Detailed Chemistry Combustion Models against Optical Diagnostic Data for Multi-Mode Combustion in a Heavy-Duty DI Diesel Engine. *Journal of Engines*, 115, 61-82.

United States Environ Protection Agency., (2002). *A Comprehensive Analysis of Biodiesel Impacts on Exhaust Emissions Draft Technical Report*. United States Environ Protection Agency. 118, doi:EPA420-P-02-001.

Wei, S., Ji, K., Leng, X., Wang, F., Liu, X. (2014). Numerical simulation on effects of spray angle in a swirl chamber combustion system of DI (direct injection) diesel engines. *Energy*. 75, 289–294.

Yang, J., Golovitchev, V.I., Redón Lurbe, P., López Sánchez, J.J. (2012). Chemical kinetic study of nitrogen oxides formation trends in biodiesel combustion. *Int J Chem Eng*. Article ID 898742, 22 pages. doi:10.1155/2012/898742.

Yang, J., Golovitchev, V.I., Naik, C.V., Meeks, E. (2013). Comparative Study of Diesel oil and Biodiesel Spray Combustion Based on Detailed Chemical Mechanisms. *J. Eng. Gas Turbines Power*. 136(3), 031401, 8 pages.

Zel'dovich, Ya.B., Sadovnikov, P.Ya., Frank-Kamenetskii, D.A. (1947). Oxidation of Nitrogen in Combustion. *Academy of Sciences of the USSR*, Moscow.

Zheng, M., Reader, G.T., Hawley, J.G. (2004). Diesel engine exhaust gas recirculation - A review on advanced and novel concepts. *Energy Convers Manag*. 45, 883–900.

Zheng, Z., Xia, M., Liu, H., Shang, R., Ma, G., Yao, M. (2018). Experimental study on combustion and emissions of n-butanol/biodiesel under both blended fuel mode and dual fuel RCCI mode. *Fuel*. 226, 240–251.

Appendix A

Measurement device specifications

Measured parameter	Device	Uncertainty characteristics
Intake air mass flow rate	Orifice plate	Uncertainty of ±2.3 kg/h
Fuel consumption	Platform balance	Uncertainty of 0.1 kg/h

Temperature in the fuel tank, ambient air, inlet air, orifice plate inlet, exhaust gas	K-type thermocouples	Measured exhaust gas with maximum uncertainty of ±11 º Other measured temperature with maximum uncertainty of ±5ºC
Cooling water temperature	PT-100 sensors	Uncertainty of ± 2ºC
Inlet air humidity	Thermo-hygrometer	Uncertainty of ± 2.5% of reading
Ambient pressure	Torricelli barometer	Resolution of ± 1.3 kPa
Engine load	Electric transducer	Uncertainty of ± 1%
Total HC emissions	Heated flame ionization detector	Resolution of ± 1 ppm
NOx emissions	Heated chemiluminescent analyzer (HCLD)	Resolution of ± 1 ppm
CO emissions	Non-dispersive infrared analyzer (NDIR)	Resolution of ± 1 ppm
CO_2 emissions	Non-dispersive infrared analyzer	Resolution of ± 0.01%
In-cylinder pressure	Piezoelectric pressure transducer – Kistler 6061B	Resolution of ± 0.5%